Terahertz quantum-cascade laser operating up to 137 K

Benjamin S. Williams, Sushil Kumar, Hans Callebaut, and Qing Hu[a)]
Department of Electrical Engineering and Computer Science and Research Laboratory of Electronics, Massachusetts Institute of Technology, Cambridge, Massachusetts 02139

John L. Reno
Sandia National Laboratories, Department 1123, MS 0601, Albuquerque, New Mexico 87185-0601

(Received 25 August 2003; accepted 24 October 2003)

We report operation of a terahertz quantum-cascade laser at 3.8 THz ($\lambda \approx 79\ \mu$m) up to a heat-sink temperature of 137 K. A resonant phonon depopulation design was used with a low-loss metal–metal waveguide, which provided a confinement factor of nearly unity. A threshold current density of 625 A/cm^2 was obtained in pulsed mode at 5 K. Devices fabricated using a conventional semi-insulating surface-plasmon waveguide lased up to 92 K with a threshold current density of 670 A/cm^2 at 5 K. © *2003 American Institute of Physics.* [DOI: 10.1063/1.1635657]

The extension of quantum-cascade laser (QCL)[1] operation from the mid-infrared into the underdeveloped terahertz frequency range (1–10 THz, 30–300 μm)[2–4] promises to provide new compact, coherent sources for applications such as spectroscopy, sensing, and imaging. At this early stage of development, high-temperature performance of terahertz QCLs is still rather limited, and cryogenic operation is required. For these lasers, the photon energy $\hbar\omega$ is smaller than the LO phonon energy ($E_{\mathrm{LO}}=36$ meV in GaAs), and nonradiative relaxation via LO-phonon scattering is suppressed for cold electron distributions. However, at higher temperatures, thermally activated LO-phonon scattering dominates the upper state lifetime τ according to $\tau^{-1}\propto\exp[(\hbar\omega - E_{\mathrm{LO}})/k_{\mathrm{B}}T_e]$, where T_e is the electron temperature. As a result, the gain in terahertz QCLs has a much stronger temperature dependence than the gain in mid-infrared QCLs, where $\hbar\omega > E_{\mathrm{LO}}$. For terahertz QCLs, operation has been obtained up to 103 K in pulsed mode and 68 K in cw mode in a bound-to-continuum design.[5,6] For chirped superlattice designs, lasing has been obtained at 74 K in pulsed mode, and 48 K in cw mode.[7] For both of these designs, depopulation of the lower radiative state takes place via intraminiband transport and scattering. High-temperature performance has been limited by various combinations of thermal backfilling of the lower radiative state from the injector, and reduction of the upper state lifetime due to thermally activated phonon scattering.

A different approach was taken for resonant phonon devices,[4,8] in which depopulation of the lower radiative state occurs via subpicosecond LO-phonon scattering. The large energy separation ($\geqslant E_{\mathrm{LO}}$) between the injector states and the lower radiative state reduces thermal backfilling. Lasing was observed in pulsed mode up to 87 K,[9] but cw operation of this first design was not obtained, due to its relatively large threshold current density ($J_{\mathrm{th}} > 800$ A/cm^2). The large J_{th} did not necessarily reflect a weak gain or high optical loss, but rather it was inflated by the presence of a strong parasitic current channel.[10]

In this letter, we report lasing up to a heat-sink temperature of $T_{\max}=137$ K in a resonant phonon structure [shown in Fig. 1(a)] that is very similar to the one reported in Ref. 4, except that the 24 Å intra-injector barrier was thickened to 30 Å. This change narrowed the 2-1 injector anticrossing from $\Delta_{21}=6.5$ meV to $\Delta_{21}=5.0$ meV. The intent was for a tighter injection doublet to provide more selective injection into the upper radiative state $n=5$. In addition, below the design bias, the thicker barrier reduces the coupling between the injector state $n=1'$ and the excited state $n=3$ in the wide well of the next module, which was the cause of the aforementioned parasitic current channel.

The structure, labeled FL178C-M1, was grown by molecular-beam epitaxy on a semi-insulating (SI) GaAs substrate with 178 cascaded modules. Cladding and contact layers were grown as in Ref. 11, except that the undoped

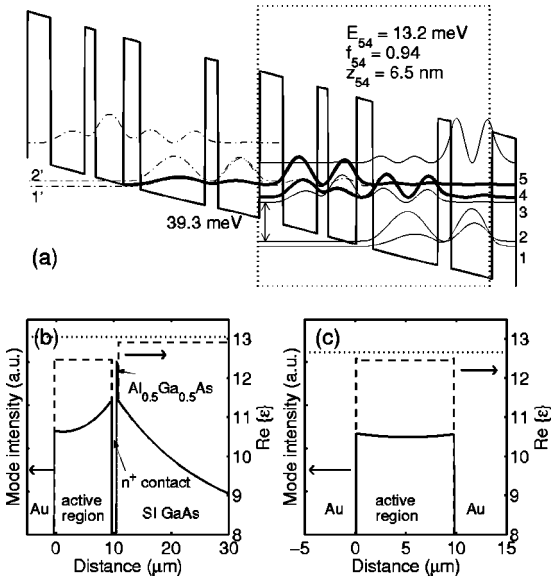

FIG. 1. (a) Conduction band profile calculated using a self-consistent Schrödinger and Poisson solver (72% band offset). The four-well module grown in GaAs/$Al_{0.15}Ga_{0.85}As$ is outlined by the dotted box. Beginning with the left injection barrier, the layer thicknesses in Å are 54/78/24/65/38/149/30/95. The 149 Å well is doped at $n=1.9\times10^{16}$ cm^{-3}, which yields a sheet density of $n=2.8\times10^{10}$ cm^{-2} per module. Also shown are the mode profiles (solid lines) and the real part of the dielectric constant $\epsilon(\omega)$ (dashed lines) for (b) SISP and (c) metal–metal waveguides.

[a)]Electronic mail: qhu@mit.edu

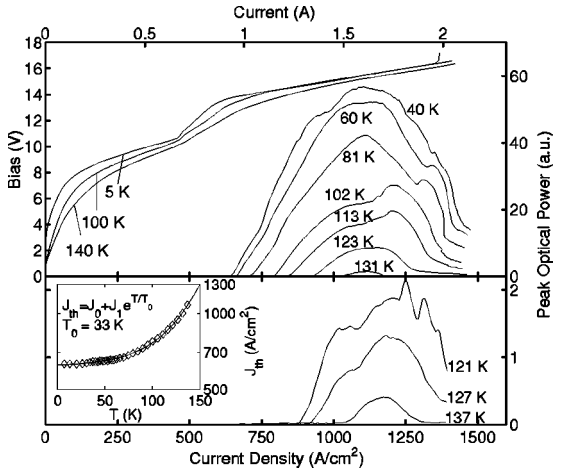

FIG. 2. Emitted light and bias versus current at various temperatures for metal–metal devices measured using 200 ns pulses repeated at 1 kHz. The $L-I$ characteristics in the upper panel are measured from a 60-μm-wide, 2.48-mm-long ridge. The $V-I$ characteristic is measured using a smaller structure (100 μm wide, 1.45 mm long). The lower panel displays $L-I$ characteristics from a 150-μm-wide, 2.74-mm-long ridge, along with its threshold current density versus temperature (inset). Note that the current axis is only applicable to the 60-μm-wide device.

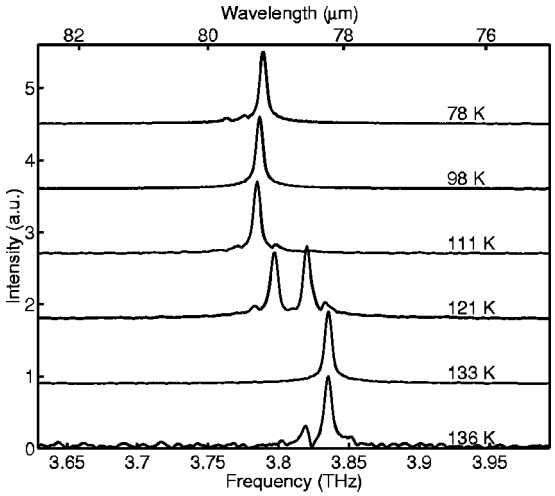

FIG. 3. Spectra from a 100-μm-wide, 2.74-mm-long metal–metal ridge taken at various heat-sink temperatures using 200 ns pulses repeated at 5 kHz, all biased at approximately the same current densities of 1170–1200 A/cm^2. A Nicolet 850 Fourier transform spectrometer was used with a Ge:Ga photodetector. The linewidth is limited by the spectrometer resolution (0.125 cm^{-1}).

$Al_{0.5}Ga_{0.5}As$ etch-stop layer was 0.3 μm thick, and the lower n^+ GaAs contact layer was 0.8 μm thick and doped at 3×10^{18} cm^{-3}. This device was fabricated into a low-loss, high-confinement metal–metal waveguide using In–Au metallic wafer bonding as described in Ref. 11, and ridges were dry etched using the top Ti/Au (200/4000 Å) metallization as a self-aligned etch mask. Devices were also processed into SI surface-plasmon (SISP) waveguides using wet etching, as described in Ref. 4. For the SISP devices only, a high-reflectivity (HR) coating (Al_2O_3/Ti/Au) was evaporated on the cleaved rear facet. One-dimensional mode profiles were calculated for the two waveguides, and are shown in Figs. 1(b) and 1(c). At 3.8 THz, a waveguide loss of $\alpha_w = 14.2$ cm^{-1} and a confinement factor of $\Gamma = 0.98$ were obtained for the metal–metal waveguide, while $\alpha_w = 8.2$ cm^{-1} and $\Gamma = 0.324$ were obtained for the SISP guide. Drude-model relaxation times of 0.1, 0.5, and 0.05 ps were used for the heavily doped semiconductor, lightly doped semiconductor, and gold, respectively.

The highest operating temperatures were observed from the metal–metal waveguide devices. Light versus current ($L-I$) characteristics taken from typical devices are shown in Fig. 2. A 150-μm-wide, 2.74-mm-long Fabry–Pérot ridge lased up to a heat-sink temperature of $T_{max}=137$ K when biased with 200 ns pulses repeated at 1 kHz. This device displayed a threshold current density of $J_{th}=625$ A/cm^2 at 5 K. In addition, a 60-μm-wide, 2.48-mm-long ridge lased up to 131 K, with $J_{th}=630$ A/cm^2 at 5 K. Voltage versus current ($V-I$) characteristics are also shown from a similar, but smaller device (100 μm wide, 1.45 mm long). In these devices, lasing occurs up to a peak current density of $\sim$1400 A/cm^2, whereupon the injector subband $n=1'$ becomes misaligned with the upper radiative state $n=5$, and negative differential resistance is observed. The shoulder in the $V-I$ at approximately 500 A/cm^2 ($\sim$10 V) corresponds to the previously mentioned parasitic current channel;[10] electrons are not injected into the upper radiative state until the device is biased beyond this point. Indeed, lasing begins at a current density only slightly higher than this parasitic channel, which indicates that J_{th} is still limited by the parasitic channel rather than by intrinsic gain or loss. Compared to the previous design, in which the lowest obtained threshold was $J_{th}=806$ A/cm^2, increasing the intra-injector barrier thickness suppressed the parasitic channel and reduced J_{th}. A plot of J_{th} versus heat-sink temperature is shown in the inset of Fig. 2, along with a fit to the phenomenological relation $J_{th} = J_0 + J_1 \exp(T/T_0)$. The extracted characteristic temperature is $T_0=33$ K. This value is significantly smaller than those for mid-infrared QCLs, which are typically greater than 100 K. Using ridges of different widths did not affect device performance very much. In addition to the devices mentioned earlier, a 100-μm-wide ridge and an 80-μm-wide ridge of the same length (2.74 mm) displayed $T_{max}=136$ and 131 K, respectively. In addition, a circular device with a 400 μm diameter lased in a whispering gallery mode with $T_{max}=105$ K.

The sharp feature in the $V-I$ associated with the parasitic channel ($\sim$10 V) is likely an indication that high-field domains have developed, and individual modules or groups of modules have ''jumped'' to higher biases to maintain constant current. This is an unintended side effect of tightening the injection doublet. Even though most modules return to their correct alignment as the bias is increased past the high differential resistance region, there is no guarantee that all modules will be correctly biased. In fact, the threshold bias voltage of $\sim$14 V is much higher than the designed value of 178×64 mV$\approx$11.4 V, which indicates that many modules are probably biased at much higher voltages than designed. Hence, injector design should be optimized to further suppress the parasitic channel and prevent high-field domain formation.

Pulsed spectra taken at up to 136 K from a 100-μm-wide, 2.74-mm-long Fabry–Pérot ridge structure are shown in Fig. 3. Lasing was seen at approximately 3.8 THz, which corresponds to a wavelength of $\lambda\approx79$ μm and a photon en-

ergy of 15.7 meV. This is somewhat higher than the 14 meV photon energy observed for the device in Refs. 4 and 9. This is consistent with high-field domain development, in which modules jump to higher bias points than they otherwise might so that the separation E_{54} is increased due to Stark shift. The observed frequency shift at different temperatures is not due to temperature tuning, but rather due to mode-hopping caused by the shift of the gain curve at slightly different bias points. The spontaneous emission linewidth is measured to be 6 meV ($\sim$1.5 THz). The line shape is far different from a Lorentzian, and this broad linewidth is likely due to non-uniform alignment of different modules.

As observed previously,[11] the metal–metal waveguide devices lased only for approximately the first 10–30 μs of an applied pulse. This is attributed to rapid heating of the active region caused by a large thermal resistance at the bonding interface. This phenomenon has been observed in similar metal–metal waveguide QCLs that operated in the mid-infrared.[12] Improvements in bonding layer quality should alleviate this problem.

Devices fabricated using SISP waveguides were also tested, but did not achieve the same high-temperature performance as their metal–metal counterparts. A 150-μm-wide, 2.97-mm-long ridge with a HR-coated rear facet obtained $T_{\max}=92$ K, with $J_{\text{th}}=670$ A/cm^2 at 5 K. A peak collected power of approximately 2.5 mW was observed in pulsed mode from a 150-μm-wide, 1.5-mm-long, HR-coated ridge. The lower $T_{\max}$ of the SISP device is primarily due to the extra loss and low confinement factor Γ. A small value of Γ inflates the effect of the mirror losses α_m, since the total threshold gain is given by $g_{\text{th}}=(\alpha_w+\alpha_m)/\Gamma$. In addition, the mirror losses are further reduced for metal–metal waveguides due to the increased facet reflectivity caused by the impedance mismatch between the tightly confined mode and free space. Current spreading in the wet-etched SISP devices may also have reduced the available gain.[9] However, heat removal for these structures was much better than for the metal–metal devices. For a 150-μm-wide, 1.5-mm-long, HR-coated ridge, cw operation was briefly observed for several seconds at 13 K before heat buildup in the cryostat stopped operation.

Monte Carlo simulations of active region transport and gain were performed as described in Ref. 10 and are consistent with the experimental results. As shown in Fig. 4, the calculated peak gain declines as the lattice temperature T_l rises above $\sim$80 K and τ_5 decreases due to thermal activation of LO-phonon scattering from $n=5$ into $n=3$ and 4. The simulation results indicate that for T_l below $\sim$80 K, the electron temperature T_e is not very sensitive to T_l, whereas above $\sim$80 K, T_e tracks T_l with a temperature difference ($\sim$20–60 K) that depends on the subband. At $T_l>80$ K, cooling due to intrasubband LO-phonon scattering becomes efficient, keeping T_e not too much above T_l.[13] From the calculated losses, which were approximated as temperature independent, we can estimate the maximum operating temperature of the laser to be $\sim$85 K for a SISP waveguide, and $\sim$160 K for a metal–metal waveguide. These values correspond reasonably well with the measured maximum temperatures of 92 and 137 K, respectively.

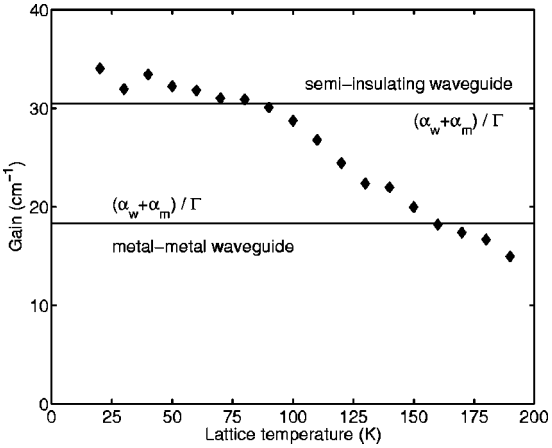

FIG. 4. Maximum available gain versus lattice temperature calculated with a Monte Carlo solver, compared with calculated threshold gain required for metal–metal and SISP waveguide.

In conclusion, we have extended the temperature range for lasing in resonant phonon terahertz QCLs by improving injection and reducing waveguide losses. Redesign of the injector region should prevent the development of high-field domains (which will result in a narrower linewidth and more modules contributing to gain), and should further reduce the parasitic current channel, which would allow lower thresholds and even higher temperature operation. Improvements in metallic wafer bonding and heat-sinking for metal–metal waveguides will allow for more robust cw operation.

The authors acknowledge R. Köhler and A. Tredicucci for helpful discussions. This work is supported by AFOSR, NASA, and NSF. Sandia is a multiprogram laboratory operated by Sandia Corporation, a Lockheed Martin Company, for the United States Department of Energy under Contract DE-AC04-94AL85000.

[1] J. Faist, F. Capasso, D. L. Sivco, C. Sirtori, A. L. Hutchinson, and A. Y. Cho, Science **264**, 553 (1994).
[2] R. Köhler, A. Tredicucci, F. Beltram, H. E. Beere, E. H. Linfield, A. G. Davies, D. A. Ritchie, R. C. Iotti, and F. Rossi, Nature (London) **417**, 156 (2002).
[3] M. Rochat, L. Ajili, H. Willenberg, J. Faist, H. Beere, G. Davies, E. Linfield, and D. Ritchie, Appl. Phys. Lett. **81**, 1381 (2002).
[4] B. S. Williams, H. Callebaut, S. Kumar, Q. Hu, and J. L. Reno, Appl. Phys. Lett. **82**, 1015 (2003).
[5] G. Scalari, L. Ajili, J. Faist, H. Beere, E. Linfield, D. Ritchie, and G. Davies, Appl. Phys. Lett. **82**, 3165 (2003).
[6] J. Faist (personal communication).
[7] R. Köhler, A. Tredicucci, F. Beltram, H. E. Beere, E. H. Linfield, A. G. Davies, D. A. Ritchie, S. S. Dhillon, and C. Sirtori, Appl. Phys. Lett. **82**, 1518 (2003).
[8] M. A. Stroscio, M. Kisin, G. Belenky, and S. Luryi, Appl. Phys. Lett. **75**, 3258 (1999).
[9] B. S. Williams, S. Kumar, H. Callebaut, Q. Hu, and J. L. Reno, Electron. Lett. **39**, 915 (2003).
[10] H. Callebaut, S. Kumar, B. S. Williams, Q. Hu, and J. L. Reno, Appl. Phys. Lett. **83**, 207 (2003).
[11] B. S. Williams, S. Kumar, H. Callebaut, Q. Hu, and J. L. Reno, Appl. Phys. Lett. **83**, 2124 (2003).
[12] K. Unterrainer, R. Colombelli, C. Gmachl, F. Capasso, H. Y. Hwang, A. M. Sergent, D. L. Sivco, and A. Y. Cho, Appl. Phys. Lett. **80**, 3060 (2002).
[13] J. Shah, in *Hot Carriers in Semiconductor Nanostructures*, edited by J. Shah (Academic, San Diego, 1992), Chap. IV.1, pp. 169–188.